Diabetologia (2018) 61:2608–2620
https://doi.org/10.1007/s00125-018-4735-7

ARTICLE

Genome-wide profiling of histone H3K27 acetylation featured fatty acid signalling in pancreatic beta cells in diet-induced obesity in mice

Takao Nammo[1] · Haruhide Udagawa[1] · Nobuaki Funahashi[1] · Miho Kawaguchi[1] · Takashi Uebanso[2] · Masaki Hiramoto[1,3] · Wataru Nishimura[1,4,5] · Kazuki Yasuda[1]

Received: 28 May 2018 / Accepted: 17 August 2018 / Published online: 3 October 2018

Abstract

Aims/hypothesis Epigenetic regulation of gene expression has been implicated in the pathogenesis of obesity and type 2 diabetes. However, detailed information, such as key transcription factors in pancreatic beta cells that mediate environmental effects, is not yet available.

Methods To analyse genome-wide *cis*-regulatory profiles and transcriptome of pancreatic islets derived from a diet-induced obesity (DIO) mouse model, we conducted chromatin immunoprecipitation coupled with high-throughput sequencing (ChIP-Seq) of histone H3 lysine 27 acetylation (histone H3K27ac) and high-throughput RNA sequencing. Transcription factor-binding motifs enriched in differential H3K27ac regions were examined by de novo motif analysis. For the predicted transcription factors, loss of function experiments were performed by transfecting specific siRNA in INS-1, a rat beta cell line, with and without palmitate treatment. Epigenomic and transcriptional changes of possible target genes were evaluated by ChIP and quantitative RT-PCR.

Results After long-term feeding with a high-fat diet, C57BL/6J mice were obese and mildly glucose intolerant. Among 39,350 islet *cis*-regulatory regions, 13,369 and 4610 elements showed increase and decrease in ChIP-Seq signals, respectively, significantly associated with global change in gene expression. Remarkably, increased H3K27ac showed a distinctive genomic localisation, mainly in the proximal-promoter regions, revealing enriched elements for nuclear respiratory factor 1 (NRF1), GA repeat binding protein α (GABPA) and myocyte enhancer factor 2A (MEF2A) by de novo motif analysis, whereas decreased H3K27ac was enriched for v-maf musculoaponeurotic fibrosarcoma oncogene family protein K (MAFK), a known negative regulator of beta cells. By siRNA-mediated knockdown of NRF1, GABPA or MEF2A we found that INS-1 cells exhibited downregulation of fatty acid β-oxidation genes in parallel with decrease in the associated H3K27ac. Furthermore, in line with the epigenome in DIO mice, palmitate treatment caused increase in H3K27ac and induction of β-oxidation genes; these responses were blunted when NRF1, GABPA or MEF2A were suppressed.

Conclusions/interpretation These results suggest novel roles for DNA-binding proteins and fatty acid signalling in obesity-induced epigenomic regulation of beta cell function.

Electronic supplementary material The online version of this article (https://doi.org/10.1007/s00125-018-4735-7) contains peer-reviewed but unedited supplementary material, which is available to authorised users.

✉ Takao Nammo
tnammo@ri.ncgm.go.jp

✉ Kazuki Yasuda
kyasuda@ri.ncgm.go.jp

[1] Department of Metabolic Disorder, Diabetes Research Center, Research Institute, National Center for Global Health and Medicine, 1-21-1 Toyama, Shinjuku-ku, Tokyo 162-8655, Japan

[2] Department of Preventive Environment and Nutrition, Institute of Biomedical Sciences, Tokushima University Graduate School, Tokushima, Japan

[3] Department of Biochemistry, Tokyo Medical University, Tokyo, Japan

[4] Department of Molecular Biology, International University of Health and Welfare School of Medicine, Narita, Chiba, Japan

[5] Division of Anatomy, Bio-imaging and Neuro-cell Science, Jichi Medical University, Shimotsuke, Tochigi, Japan

Research in context

What is already known about this subject?

- Environmental factors, such as dietary habits and a sedentary lifestyle, are closely related to onset and progression of obesity and type 2 diabetes
- Susceptibility variants for common diseases, including type 2 diabetes, have been identified mainly in non-coding regions of the genome, and some variants induce changes in local chromatin structures
- Epigenetic modifications caused by changes in the extracellular environment critically influence the cellular response to various physiological and pathological conditions

What is the key question?

- Are specific DNA-binding motifs and their corresponding transcription factors involved in the alterations of critical molecular functions in pancreatic beta cells via epigenetic mechanisms under obesogenic environments?

What are the new findings?

- Genome-wide profiling of histone H3 lysine 27 acetylation revealed that high-fat-diet feeding resulted in global changes of the epigenetic state in pancreatic islets of mice
- Novel DNA-binding motifs and their corresponding transcription factors, including NRF1, GABPA and MEF2A, were identified by de novo motif search
- The identified transcription factors were involved in the regulation of genes critical for fatty acid β-oxidation under palmitate treatment

How might this impact on clinical practice in the foreseeable future?

- This helps our understanding of pathological cellular states and suggests that transcription factor-mediated epigenetic modulation of beta cells could be a potential intervention for obesity and type 2 diabetes

Data availability The next-generation sequencing data in the present study were deposited at ArrayExpress.

RNA-Seq:

Dataset name: ERR2538129 (Control), ERR2538130 (Diet-induced obesity)

Repository name and number: E-MTAB-6718 - RNA-Seq of pancreatic islets derived from mice fed a long-term high-fat diet against chow-fed controls.

ChIP-Seq:

Dataset name: ERR2538131 (Control), ERR2538132 (Diet-induced obesity)

Repository name and number: E-MTAB-6719 - H3K27ac ChIP-Seq of pancreatic islets derived from mice fed a long-term high-fat diet (HFD) against chow-fed controls.

Keywords Epigenetics · Fatty acid oxidation · Glucose intolerance · High-fat diet · Histone acetylation · Insulin secretion · Next-generation sequencing · Obesity · Pancreatic islets · Transcriptome · Type 2 diabetes

Abbreviations

ChIP	Chromatin immunoprecipitation
ChIP-Seq	Chromatin immunoprecipitation coupled with high-throughput sequencing
DAVID	The Database for Annotation, Visualization and Integrated Discovery
DIO	Diet-induced obesity
FOXA1	Forkhead box A1
GABPA	GA repeat binding protein α
GEO	Gene Expression Omnibus
GSIS	Glucose-stimulated insulin secretion
GWAS	Genome-wide association study (studies)
H3K27ac	Histone H3 lysine 27 acetylation
HFD	High-fat diet
HNF1	HNF1 homeobox A
HOMER	Hypergeometric Optimization of Motif EnRichment
IPGTT	Intraperitoneal glucose tolerance test
KEGG	Kyoto Encyclopedia of Genes and Genomes
MAFK	v-maf musculoaponeurotic fibrosarcoma oncogene family protein K
MEF2A	Myocyte enhancer factor 2A

NRF1	Nuclear respiratory factor 1
qPCR	Quantitative PCR
RFXDC2	Regulatory factor X, 7
RNA-Seq	High-throughput RNA sequencing
SICER	Spatial clustering for identification of ChIP-enriched regions
TSS	Transcription start site

Introduction

Type 2 diabetes and obesity are chronic metabolic disorders that affect an increasing number of people globally [1, 2]. Genome-wide association studies (GWAS) [3] have highlighted the role of *cis*-regulatory elements in various disease processes by combining knowledge of comprehensive epigenetic profiling [4–6]. However, given the modest effect of identified susceptibility variants, achieving a full understanding of a disease remains challenging [3].

There is clear evidence supporting the role of environmental factors in type 2 diabetes [1, 2, 7]. Obesity, along with reduced physical activity, is regarded as being responsible for the recent pandemic [7]. Insufficient insulin secretion is essential in the development of type 2 diabetes, and a variety of environmental factors as well as genetic predisposition play important roles in the modification of beta cell function [7].

Much remains unknown, especially in humans, about the molecular characteristics of the pancreatic islets of Langerhans under various physiological and pathological conditions [8]. Several studies have provided new insights through more comprehensive analyses [4, 9–11]. Among assays for epigenomic profiling, histone H3 lysine 27 acetylation (H3K27ac), a marker of active regulatory regions [12], is recognised as being valuable not only in annotating human variants [6] but also in providing information on diseased tissue from both humans and mice [13, 14].

Changes in epigenetic modifications and transcriptional regulation are essential for phenotypic adaptation of cell types to environments, including high-fat diet (HFD) [15–17]. Since some DNA-binding proteins play a role in triggering epigenetic reprogramming in specific genomic regions [18], we hypothesised that the corresponding sequence motifs could be enriched in *cis*-regulatory regions with local epigenetic alterations in response to environmental stimuli. In the present study, by examining genome-wide H3K27ac signatures and whole transcriptome, we aimed to identify sequence motifs enriched in genomic regions exhibiting HFD-driven epigenetic changes in mouse pancreatic islets. In addition, we investigated the involvement of DNA-binding proteins in the regulation of gene expression and pancreatic beta cell function during the development of obesity and glucose intolerance.

Methods

Mice and metabolic assessment Male C57BL/6JJcl mice were purchased from CLEA Japan (Tokyo, Japan). Half of the mice were switched from a standard chow diet (CE-2; CLEA Japan) to an HFD (D12492, 60% fat; Research Diets, New Brunswick, NJ, USA) at 10 weeks of age. The samples were not randomised by statistical computing. Mice were weighed to the nearest 0.1 g. Blood glucose was determined by tail-vein bleeding. Following fasting of the mice overnight, an intraperitoneal glucose tolerance test (IPGTT) was conducted using a glucose dose of 1 g/kg body weight. Plasma was separated by centrifugation of whole blood at an ambient temperature of 22 ± 2°C and frozen in liquid nitrogen for measurement of insulin levels using a Mouse Insulin ELISA Kit (Morinaga Institute of Biological Science, Kanagawa, Japan). All animal procedures at the National Center for Global Health and Medicine were approved by the Institutional Animal Care and Use Committee. Blinding for experimenters was not carried out. We did not lay down any criteria for inclusion and exclusion of any data, since all the results supported the main findings of the study. For details, see electronic supplementary material (ESM) Methods.

Isolation of pancreatic islets Pancreatic islets were isolated from anaesthetised 37-week-old mice as described [19]. See ESM Methods for details.

High-throughput RNA sequencing Total RNA was extracted from pancreatic islets using Trizol (Thermo Fisher Scientific, Waltham, MA, USA). Library preparation was performed using the TruSeq Stranded Total RNA Sample Prep Kit (Illumina, San Diego, CA, USA) and high-throughput RNA sequencing (RNA-Seq) was performed using the Illumina HiSeq 2000 platform with 100 bp paired-end sequencing. See ESM Methods for details.

Analysis of differential gene expression and functional annotation Analyses were performed using DESeq 1.32.0 [20] with an iterative pipeline (iterative differentially expressed gene elimination strategy [iDEGES]/DESeq) [21], both of which were R/Bioconductor packages (https://www.bioconductor.org/). Reads per million (RPM)-normalised read counts allowed the visualisation of global changes in gene expression as an MA plot. For those genes with highest variance ($p < 0.1$), functional annotation was analysed using the Database for Annotation, Visualization and Integrated Discovery (DAVID) 6.8 (https://david.ncifcrf.gov/, accessed 15 Feb 2018) [22]. See ESM Methods for details.

Chromatin immunoprecipitation, high-throughput sequencing and analysis of differential sequencing signals Chromatin preparation for chromatin immunoprecipitation (ChIP) was performed as described in [4] with modifications. A list of the

primary antibodies used is provided in ESM Table 1. ChIP libraries were prepared using NEBNext ChIP-Seq Library Prep Master Mix Set for Illumina (New England BioLabs, Ipswich, MA, USA) and were sequenced on a HiSeq 2000 system (Illumina). The processed data were uploaded to the Integrative Genomics Viewer (IGV) browser 2.3.75 (http://software.broadinstitute.org/software/igv/) [23]. Spatial clustering for identification of ChIP-enriched regions (SICER) v1.1 [24] was used to compare differentially enriched regions between experimental and control groups using the command SICER-df-rb.sh. Running this command enabled identification of significantly enriched H3K27ac regions in each library, merging of all overlapping intervals and determination of the significance of changes by comparing the signal intensity of ChIP coupled with high-throughput sequencing (ChIP-Seq) in HFD samples with that in controls on each merged H3K27ac region. To identify DNA sequence motifs enriched in merged H3K27ac regions with HFD-induced changes, we used Hypergeometric Optimization of Motif EnRichment (HOMER) v4.6 (http://homer.ucsd.edu/homer/) [25] for de novo motif detection using the whole genome as the background by running the command findMotifsGenome.pl. This command is a tool used to identify binding motifs enriched in the genomic intervals without prior knowledge of the transcription factor binding sites. First, analyses were performed according to the default parameters for base redundancy and motif length (8, 10 or 12 bp). Subsequently, the identified motifs were checked for homology with known motif matrices and the best match result was presented as a likely candidate, which we listed in our tables. See ESM Methods for details.

Correlating differential H3K27ac signals with differential gene expression Each H3K27ac region was mapped to the closest gene based on distance to the transcription start site (TSS), as described [14]. Overall *cis*-regulatory activity of individual genes was defined as increased, decreased or unchanged by counting the number of regions showing increased H3K27ac relative to regions showing a decrease. DESeq2 1.20.0 [26] enabled comparison of $\log_2$ (fold change) between categories. For Kyoto Encyclopedia of Genes and Genomes (KEGG) pathway analysis [27], we selected the 610 most upregulated and 174 most downregulated genes, which also showed overall increases and decreases in *cis*-regulatory activity, respectively. See ESM Methods for details.

Cell culture and insulin secretion measurements in INS-1 cells and pancreatic islets INS-1 cells (a rat beta cell line) were gift from C. B. Wollheim (Lund University; University of Geneva) and N. Sekine (University of Geneva), and were cultured as described [19]. Batch insulin release was estimated by incubating in 3 mmol/l glucose, 25 mmol/l glucose or 30 mmol/l KCl for 60 min. For pancreatic islets isolated from 54-week-old mice, insulin secretion in 2.8 mmol/l glucose, 16.7 mmol/l glucose or 60 mmol/l KCl in 30 min batch incubations was measured as described [19]. Total insulin content was calculated by summating the insulin secreted into the medium with the amount of insulin measured by whole-cell extraction with acid ethanol for 24 h at 4°C. Insulin secretion was expressed as a percentage of the total insulin content. For INS-1 cells, insulin was detected using a Mouse Insulin ELISA Kit (AKRIN-011 T; Shibayagi, Gunma, Japan). Mycoplasma contamination was not tested. See ESM Methods for details.

siRNA knockdown of NRF1, GABPA and MEF2A followed by palmitate treatment Lipofectamine 2000 (Thermo Fisher Scientific) was used for reverse transfection of specific siRNAs in INS-1 cells (ESM Table 2). Palmitate (Wako Pure Chemical Industries, Osaka, Japan), sodium palmitate (Sigma-Aldrich, St Louis, MO, USA) or vehicle treatment began 36 h after siRNA-mediated knockdown, and treated cells were used for the following experiments after incubation for 48 h. See ESM Methods for details.

Quantitative real-time PCR Quantification of cDNA or ChIP-DNA samples was conducted via standard quantitative PCR (qPCR) methods using SYBR Green (Thermo Fisher Scientific). The following genes were tested: *Acaa2*, *Gabpa*, *Mef2a*, *Nrf1* and *Slc25a20* for rat cDNA; *Acaa2*, *Cpt1a*, *Elovl6*, *Fads2*, *Mki67*, *Scd2*, *Slc25a20* and *Top2a* for mouse cDNA and *Acaa2* and *Slc25a20* for rat ChIP-DNA. A list of primers is provided in ESM Table 3. See ESM Methods for details.

Statistics We used R or GraphPad Prism 7.04 (GraphPad Software, San Diego, CA, USA) for statistical analyses. The two-sided unpaired *t* tests, two-sided paired *t* tests, or Mann–Whitney *U* tests were applied. Error bars in the Figures represent SD.

Accession numbers Previous ChIP-Seq data in human or mouse tissues were obtained from Gene Expression Omnibus (GEO) and processed as described above (summarised in ESM Table 4). The UCSC liftOver tool and Ensembl Compara cross-species resources (https://www.ensembl.org/info/genome/compara/index.html) were applied for conversion of genomic positions between reference genomes mm9, hg19 and rn6. Data in the present study were deposited at ArrayExpress under accession number E-MTAB-6718 (RNA-Seq) and E-MTAB-6719 (ChIP-Seq).

Results

Body weight and glucose tolerance in mouse model of diet-induced obesity To investigate the mechanisms by which environmental factors induce phenotypic differences in

pancreatic beta cells, a diet-induced obesity (DIO) model was employed, using male C57BL/6J mice [28]. The HFD was started at 10 weeks of age (Fig. 1a). The initial 4 weeks of HFD feeding resulted in a slight but significant increase in average body weight (control mice 27.0 ± 2.05 g vs DIO mice 29.2 ± 3.04 g, $p < 0.01$, ESM Fig. 1a) and non-fasting blood glucose level (control mice 9.19 ± 1.6 mmol/l vs DIO mice 10.1 ± 1.6 mmol/l, $p < 0.05$, ESM Fig. 1b). IPGTT showed that glucose tolerance was impaired in DIO mice, although these mice displayed enhanced glucose-stimulated insulin secretion (GSIS) at 15 min post-glucose injection (ESM Fig. 1c,d). Thereafter, mildly higher non-fasting blood glucose levels were sustained in DIO mice for 37 weeks of HFD feeding (total age 47 weeks; Fig. 1a–c). During IPGTT, DIO mice showed mild glucose intolerance (Fig. 1d) and hyperinsulinaemia both at baseline (8.8-fold, $p < 0.01$; Fig. 1e) and at 15 min post-glucose injection (7.5-fold, $p < 0.01$; Fig. 1e).

Impact of long-term HFD feeding on pancreatic islet transcriptome To clarify the global relationships between epigenome and transcriptome in the pancreatic islets after HFD feeding for an extended period of 27 weeks, we used a next-generation sequencing platform (Fig. 1a and ESM Fig. 2). RNA-Seq analyses were performed by generating approximately 31.7–35.1 million high-quality paired-end sequencing reads (ESM Table 5).

To identify genes differentially expressed between DIO and control mice, we chose DESeq [20] with an iterative pipeline [21] for read count normalisation and gene ranking. The analysis revealed that most genes showed relatively limited dynamics with respect to the read count ratio (ESM Fig. 3a). Nevertheless, analysis of the top-ranked 303 upregulated genes ($p < 0.1$) (ESM Fig. 3b and ESM Tables 6, 7) using DAVID [22] revealed enrichment of terms that were linked to islet functions important for adaptive responses to HFD, including the endoplasmic reticulum [29] (ESM Fig. 3b and ESM Table 7).

We also performed the same analysis on the top-ranked 269 downregulated genes ($p < 0.1$) (ESM Fig. 3c and ESM Tables 6, 8). Interestingly, the enriched terms were mainly related to epigenetic regulation of gene transcription, which may suggest the involvement of epigenetic change in pancreatic islets following prolonged HFD feeding (ESM Fig. 3c and ESM Table 8).

Genome-wide changes in H3K27ac associated with differential gene expression under HFD feeding H3K27ac ChIP-Seq was used for genome-wide identification of active *cis*-regulatory elements in the pancreatic islets (ESM Fig. 2). Approximately 88% of 43.8–49.6 million reads were aligned to the mouse reference genome (ESM Table 9). Using SICER [24], we determined 37,534 and 40,207 H3K27ac-enriched regions genome-wide for control and DIO libraries with median size of 3.6 kb and 3.2 kb (ESM Tables 10, 11), respectively, further generating a catalogue of 39,350 merged regions as putative *cis*-regulatory regions shared between our samples with median size of 3.8 kb (Fig. 2a, ESM Fig. 2 and ESM Table 12).

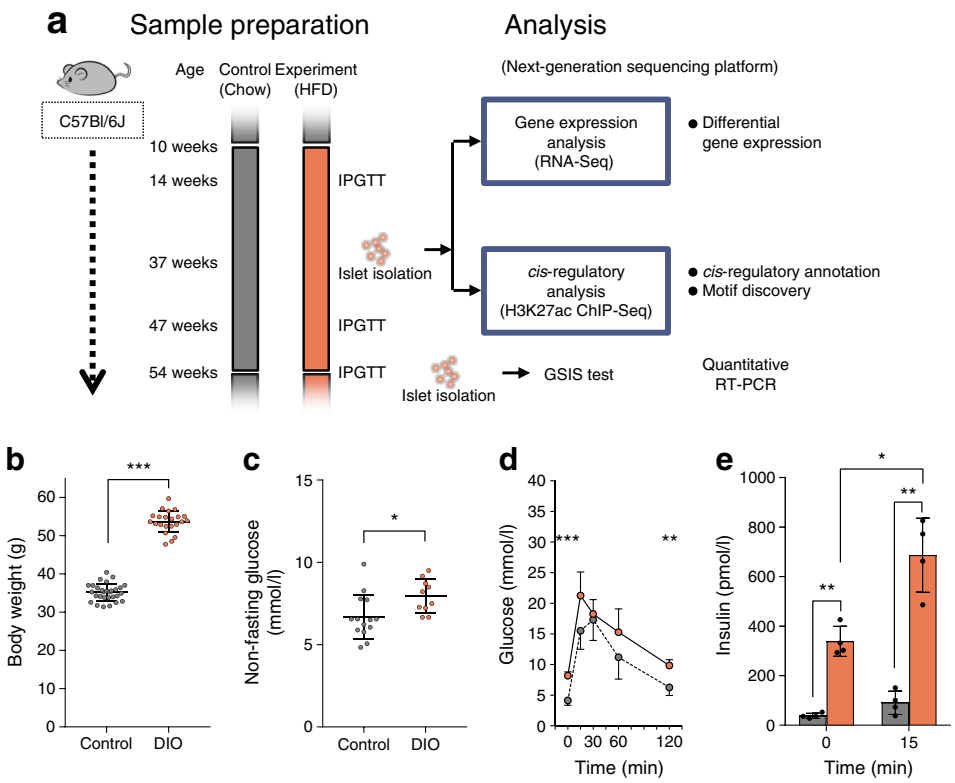

Fig. 1 Generation and characterisation of DIO mice. (**a**) The time course diagram and analytical strategies. (**b**–**e**) Metabolic assessment of 47-week-old mice (after completing 37 weeks of HFD feeding), showing body weight (**b**; $n = 29$ for control group and $n = 22$ for DIO group), non-fasting blood glucose (**c**; $n = 14$ for control group and $n = 10$ for DIO group), IPGTT glucose excursion (**d**; grey circles, control, $n = 4$; orange circles, DIO, $n = 4$) and IPGTT plasma insulin values (**e**; grey bars, control, $n = 4$; orange bars, DIO, $n = 4$). Data are means ± SD. *$p < 0.05$, **$p < 0.01$ and ***$p < 0.001$ (in **d**, DIO vs control at specific timepoint)

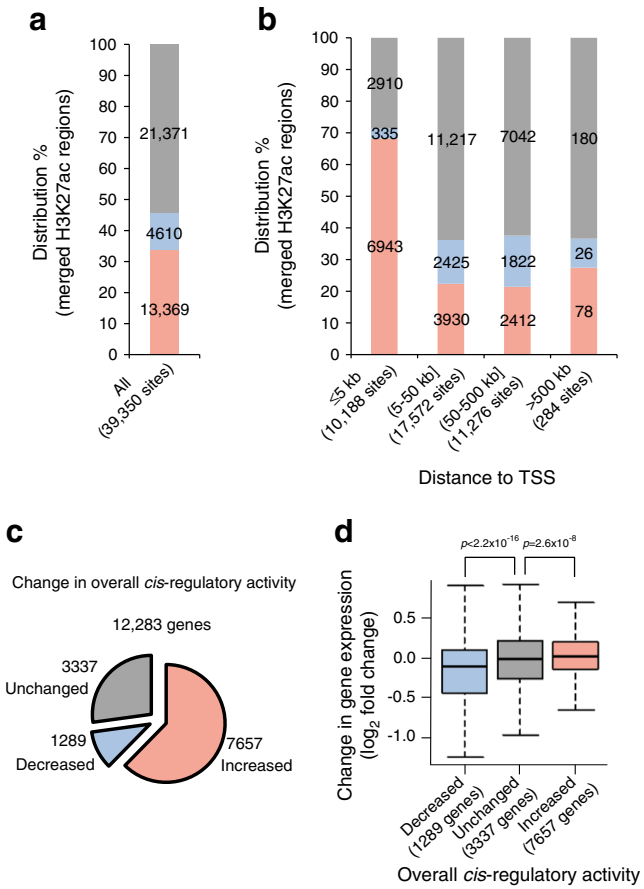

Fig. 2 RNA-Seq and H3K27ac ChIP-Seq analysis of pancreatic islets derived from DIO mice. (**a**) Bar plot showing the number of merged H3K27ac regions that were increased, decreased or unchanged upon HFD feeding. (**b**) Genomic distribution of H3K27ac regions showing HFD-induced changes in ChIP-Seq signal intensity for regions in ≤5 kb, 5–50 kb, 50–500 kb and > 500 kb distance from TSSs. Pink bars, increased H3K27ac sites; blue bars, decreased H3K27ac sites; grey bars, unchanged H3K27ac sites. (**c**) Pie chart indicating the number of genes associated with *cis*-regulatory regions, where the direction of change in *cis*-regulatory activity as a whole was regarded to be increased, decreased or unchanged. Only genes that could be tested for differential gene expression by DESeq were included. Data without knowledge of DESeq results are shown in ESM Fig. 5b. (**d**) Box plot showing differential expression of genes associated with *cis*-regulatory elements, the overall activity of which was decreased, unchanged and increased. The horizontal line inside the box is the median value. The upper and lower ends of the box are the 75th and 25th percentile for values, respectively. The vertical lines from the ends of the box (whiskers) represent the smallest or largest observed values within 1.5 times the interquartile range. *p* values were calculated using the Mann–Whitney *U* test

SICER also detected changes in the ChIP-Seq signal in individual merged regions [24]. We found 13,369 increased and 4610 decreased H3K27ac regions in the islets derived from DIO mice (Fig. 2a, ESM Fig. 2 and ESM Table 12), with median fold changes in normalised enrichment of 1.30 (first quartile 1.20, third quartile 1.41) and 0.73 (first quartile 0.67, third quartile 0.80), respectively. Compared with unchanged and decreased H3K27ac, we found that increased H3K27ac showed a greater distribution in the promoter-proximal regions (Fig. 2b and ESM Fig. 4a–d). Of all the H3K27ac regions, increased H3K27ac accounted for 68.1% (6943/10,188) from −5 kb to +5 kb relative to the TSS (Fig. 2b), while it accounted for less than 22.0% (6420/29,132) if located >5 kb relative to the TSS (Fig. 2b).

To connect epigenetic changes with the transcriptome, a precise regulatory map of the cell types is vital [30]. In the present study, however, we assigned a single gene to each merged H3K27ac region using only genomic positioning information (termed a 'single nearest gene association rule' in the Genomic Regions Enrichment of Annotations Tool [GREAT] [31]). A similar approach was also employed in a previous study that successfully analysed a mouse model of Alzheimer's disease [14]. Accordingly, expression of 9391 and 2794 genes were assumed to be associated with increased and decreased H3K27ac, respectively (ESM Table 6 and ESM Fig. 5a).

As 13.3% (1632/12,283) of all H3K27ac-harbouring genes revealed regulatory regions consisting of both increased and decreased H3K27ac (ESM Fig. 5c and ESM Table 6), we investigated how changes in individual gene expression arose according to the number of increased H3K27ac sites relative to those decreased (Fig. 2c,d and ESM Fig. 5b). Compared with genes containing equal numbers of increased and decreased H3K27ac regions, the median $\log_2$ fold change in gene expression was significantly larger when the increased H3K27ac was superior in number in the *cis*-regulatory domain ($p = 2.6 \times 10^{-8}$; Fig. 2d), whereas it was significantly smaller when the number of increased H3K27ac regions was less than the decreased ones ($p < 2.2 \times 10^{-16}$; Fig. 2d).

De novo motif analysis of HFD-responsive H3K27ac regions revealed enrichment of novel DNA-binding sites We sought to determine sequence motifs for DNA-binding proteins that were significantly enriched in differentially enriched H3K27ac regions by HOMER [25], the de novo motif analysis (ESM Fig. 2). Increased H3K27ac in the islets of DIO mice revealed a significant enrichment for 12 motifs (threshold, $p < 1 \times 10^{-12}$; Table 1), including binding motifs for known transcription factors, such as regulatory factor X, 7 (RFXDC2) [32], forkhead box A1 (FOXA1) [33] and HNF1 homeobox A (HNF1) [34]. However, the analysis also revealed highly enriched motifs exhibiting a close match to the consensus sequences for nuclear respiratory factor 1 (NRF1), GA repeat binding protein α (GABPA) and myocyte enhancer factor 2A (MEF2A) (all with score > 0.900; Table 1), the biological relevance of which had not been well described for beta cells. Further, these motifs were not detected either in unchanged or decreased H3K27ac regions (ESM Tables 13 and 14). We found that there were 3168 NRF1, 3281 GABPA and 1366 MEF2A motifs in 2369, 2555 and 1207 increased H3K27ac regions, respectively. These regions were further connected to

Table 1 De novo motif discovery by HOMER in HFD-responsive H3K27ac regions

Transcription factor	Score	*p* value	Motif	No. of motifs in increased H3K27ac regions	No. of increased H3K27ac regions including this motif	No. of assigned genes
ZFP410	0.633	1×10^{-56}		39,529	7924	7305
NRF1	0.973	1×10^{-42}		3168	2369	2318
GABPA	0.974	1×10^{-40}		3281	2555	2497
YY1	0.864	1×10^{-39}		1436	1282	1252
GFY(?)[a]	0.986	1×10^{-32}		1825	1529	1483
RFXDC2	0.597	1×10^{-31}		19,274	6723	6322
MEF2A	0.926	1×10^{-25}		1366	1207	1113
SP2	0.530	1×10^{-23}		2049	1675	1659
FOXA1	0.931	1×10^{-15}		2893	2281	2045
HNF1	0.895	1×10^{-13}		1010	916	879
RUNX	0.670	1×10^{-13}		2191	1822	1695
NFIL3	0.873	1×10^{-13}		778	738	726

Analysis using HOMER for increased H3K27ac regions revealed 12 significant motifs, including NRF1, GABPA and MEF2A. The table also includes data about the number of de novo sequence motifs identified in increased H3K27ac regions in DIO mice and the total number of genes assigned to increased H3K27ac regions containing these motifs. GFY, general factor Y; NFIL3, nuclear factor, interleukin 3 regulated; RUNX, runt related transcription factor; SP2, Sp2 transcription factor; YY1, YY1 transcription factor; ZFP410, zinc finger protein 410

[a] The principal factors that bind this motif have not been identified. See http://homer.ucsd.edu/homer/motif/motifDatabase.html

2318, 2497 and 1113 putative target genes, respectively (Table 1). We found only one motif for v-maf musculoaponeurotic fibrosarcoma oncogene family protein K (MAFK) in decreased H3K27ac, with moderate significance (score = 0.617, $p = 1 \times 10^{-14}$; ESM Table 13).

NRF1 and GABPA are involved in local epigenomic regulation in INS-1 cells of the palmitate-induced expression of *Acaa2* and *Slc25a20* for β-oxidation Next, we tested how these transcription factors could be involved in the regulation of H3K27ac and gene expression, especially under an environmental condition mimicking DIO mice. Within the HFD model, the exogenous factors triggering epigenomic modifications to specific genomic loci in beta cells are very important. There are many possible candidates but among them we examined the role of NEFA using INS-1 cells, a rat beta cell line. Since our data suggested that the regulatory effect of H3K27ac was not always strong (Fig. 2d), we first selected the most variable 1000 genes that were either upregulated or downregulated (Fig. 3). Among them, we found that 610 upregulated and 174 downregulated genes also exhibited a change in the overall H3K27ac in the same direction (ESM Fig. 6a,b). To obtain functional insights into these distinct gene sets, we performed KEGG-based pathway analysis [27]. Among various enriched metabolic pathways (ESM Tables 15, 16), those related to fatty acid metabolism (degradation and biosynthesis of fatty acids) were identified both in upregulated and downregulated genes, respectively (Fig. 3, Table 2 and ESM Tables 15, 16). These findings prompted us to focus on two genes, *Acaa2* and *Slc25a20*; both are involved in mitochondrial fatty acid β-oxidation and have been reported to be upregulated in the presence of high NEFA levels [35–37]. Furthermore, previous ChIP-Seq data suggested that binding of NRF1 and GABPA to their binding motifs was located close to the TSSs of *Acaa2* and *Slc25a20* (Fig. 4a,b, ESM Fig. 7), respectively.

We investigated the effects of 0.5 mmol/l palmitate on the epigenome, as well as the expression of *Acaa2* or *Slc25a20* in INS-1 cells, in the presence or absence of the siRNA-mediated knockdown of either NRF1 or GABPA (Fig. 5). *Nrf1* siRNA and *Gabpa* siRNA treatment reduced mRNA levels by 35% ($p < 0.001$; Fig. 5a) and 46% ($p < 0.001$; Fig. 5e), respectively. At 48 h after palmitate treatment, we found that mRNA levels of *Acaa2* and *Slc25a20* in INS-1 cells increased approximately 6.1-fold ($p < 0.01$; Fig. 5b) and 2.6-fold ($p < 0.001$; Fig. 5f) compared with the vehicle-treated control, respectively. Although ChIP-qPCR revealed NRF1 and GABPA binding to expected sites containing their binding motifs (Fig. 4a,b and ESM Fig. 8a,c), enhanced binding was not observed after palmitate treatment (Fig. 5c,g and ESM Fig. 8a,c). However, suppression of binding for each of these transcription factors by siRNA-mediated knockdown resulted in significant downregulation of both *Acaa2* (1.95-fold, $p < 0.001$; Fig. 5b) and

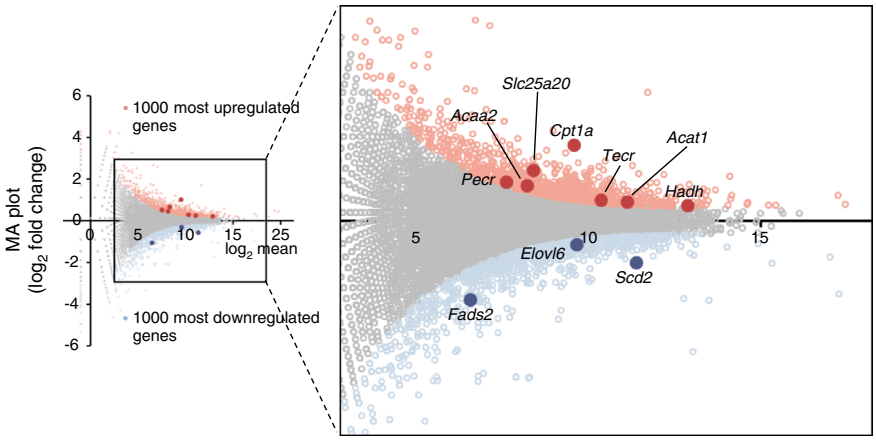

Fig. 3 MA plot for differential analysis of gene expression between DIO and control samples using DESeq. The plots for selected genes are represented in red or dark blue. The light red or light blue represent the 1000 top-ranked genes that exhibited upregulation or downregulation, respectively, facilitating the identification of genes with higher variance. A zoomed image is also presented

Slc25a20 (1.45-fold, $p < 0.05$; Fig. 5f), indicating that they were direct targets of NRF1 and GABPA, respectively. Although palmitate allowed a similar increase in mRNA levels under knockdown conditions (sevenfold increase in *Acaa2* under NRF1 knockdown, $p < 0.001$, Fig. 5b; 2.9-fold increase in *Slc25a20* under GABPA knockdown, $p < 0.01$, Fig. 5f), the resultant mRNA levels were about 59.2% ($p < 0.01$; Fig. 5b) and 77.7% ($p < 0.05$; Fig. 5f) of the values observed when the INS-1 cells were treated with both scrambled siRNA and palmitate. Thus, NRF1 and GABPA were involved in the expression of *Acaa2* and *Slc25a20*, respectively, both at baseline and following palmitate treatment.

For epigenetic analysis, we measured H3K27ac enrichment using qPCR primer sets for *cis*-regulatory elements of interest (Fig. 4, ESM Fig. 7 and ESM Table 3). Within the regions corresponding to the islet-merged H3K27ac regions spanning the TSS, H3K27ac enrichment in *Acaa2* and *Slc25a20* was lower than the control by 37.6% ($p < 0.05$; Fig. 5d and ESM Fig. 8b) and 28.8% ($p < 0.05$; Fig. 5h and ESM Fig. 8d) upon knockdown of NRF1 and GABPA, respectively. As observed in quantitative RT-PCR analysis of *Acaa2* or *Slc25a20* transcripts (Fig. 5b,f), ChIP-qPCR showed that the increase in H3K27ac in response to palmitate was blunted by knockdown of NRF1 and GABPA, respectively (Fig. 5d,h and ESM Fig. 8b,d), although the fold change in H3K27ac enrichment before and after palmitate treatment was similar regardless of whether NRF1 or GABPA was suppressed by siRNA. H3K27ac of *Acaa2* increased in scrambled-siRNA-treated cells by 2.43-fold ($p < 0.01$), whereas it increased in *Nrf1*-siRNA-treated cells by 2.57-fold ($p < 0.01$) (Fig. 5d and ESM Fig. 8b). Although palmitate increased H3K27ac in *Slc25a20* by 1.46-fold in control cells ($p < 0.05$; Fig. 5h and ESM Fig. 8d), a significant increase was not observed when GABPA was suppressed (Fig. 5h and ESM Fig. 8d).

MEF2A regulated fatty acid β-oxidation genes, *Acaa2* and *Slc25a20*, similarly to NRF1 and GABPA Further, we tested whether MEF2A regulated *Acaa2* and *Slc25a20*. Rather than a localised peak, the TSS regions of *Acaa2* and *Slc25a20* genes revealed modest and relatively broad signals in previously deposited MEF2A ChIP-Seq data (ESM Fig. 7). Treatment of INS-1 cells with *Mef2a* siRNA resulted in a reduction in mRNA level of 18.8% ($p < 0.01$; Fig. 5i). The downregulation of *Acaa2* and *Slc25a20* was not significant following MEF2A knockdown (Fig. 5j,k). However, MEF2A knockdown resulted in 26.7% ($p < 0.05$) and 30.1% ($p < 0.01$) decrease in expression of *Acaa2* and *Slc25a20*, respectively, in the presence of palmitate treatment (Fig. 5j,k). Taken together, these results suggest the important roles of the transcription factor motifs and their binding transcription factors in the regulation of genes and epigenome for fatty acid β-oxidation.

Knockdown of binding transcription factors for enriched motifs resulted in increased basal insulin secretion in INS-1 cells To gain insight into the functional effects of increased H3K27ac containing the above-described motifs on beta cells, we performed GSIS tests in INS-1 cells treated with *Nrf1*, *Mef2a* or *Gabpa* siRNA. For *Nrf1*, besides cells treated with siRNA and vehicle, we also tested GSIS for knockdown cells that were treated with 0.5 mmol/l palmitate for 48 h to observe the effect of environmental load on cells with impaired regulation of motif-mediated transcription (Fig. 6a,d). Compared

Table 2 KEGG pathway enrichment of differentially expressed genes that were accompanied by H3K27ac change in the same direction

Differential expression	KEGG pathway	Genes	Fold enrichment	*p* value
Upregulated	Fatty acid metabolism	*Acaa2*, *Pecr*, *Hadh*, *Acat1*, *Tecr*, *Cpt1a*	3.35	0.032
Downregulated	Biosynthesis of unsaturated fatty acids	*Scd2*, *Fads2*, *Elovl6*	14.1	0.018

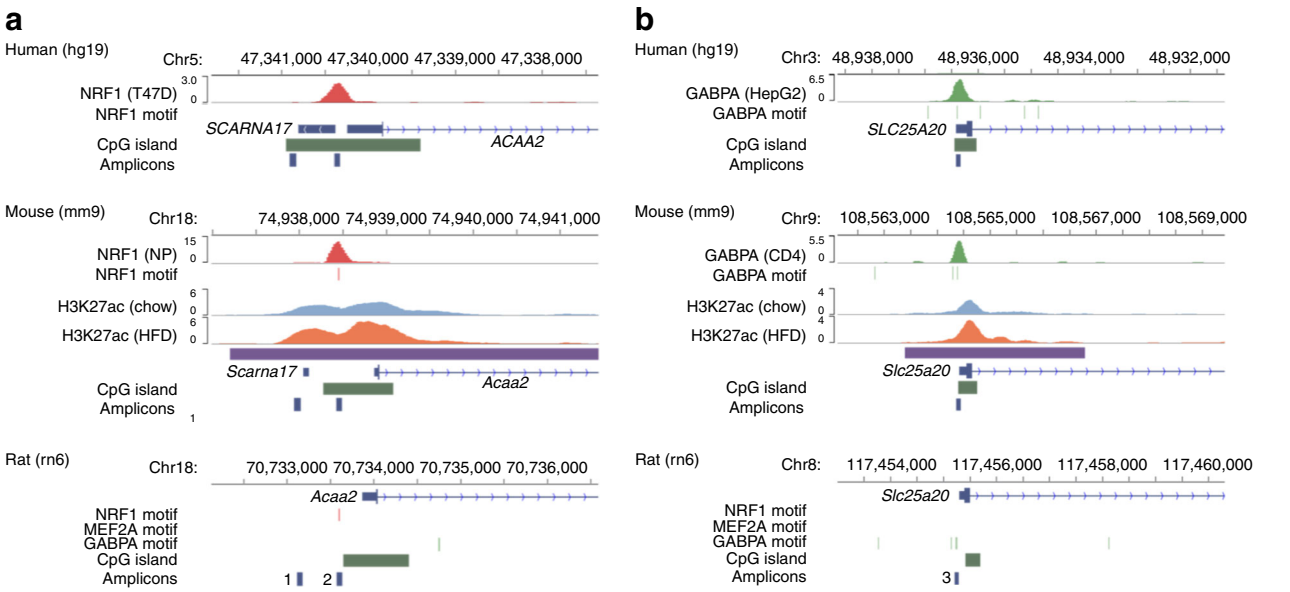

Fig. 4 Profiles of islet H3K27ac in the *Acaa2* and *Slc25a20* loci and the inference of NRF1 and GABPA binding sites, respectively, from previously deposited ChIP-Seq data. H3K27ac ChIP-Seq profiles are shown for control (light blue) and experimental DIO (orange) mice; purple bars track H3K27ac increases in the experimental data. Previously deposited ChIP-Seq data for NRF1 (red) or GABPA (light green) are also included, together with vertical lines for the DNA-binding motifs. CpG islands and qPCR products are represented by dark green and dark blue bars, respectively. To show the evolutionary conservation of the locus, panels for human (hg19), mouse (mm9) and rat (rn6) are arranged vertically. Scale bars represent the coverage expressed as read counts normalised per million reads. For further information, including the results of other cell types and MEF2A ChIP-Seq, see ESM Fig. 7. (**a**) The *Acaa2* locus showed an increase in H3K27ac surrounding the TSS, which was HFD responsive. A conserved NRF1 motif was found within this region in both mice and rats but not in humans, due to a single base-pair substitution. Mice showed a strong and localised binding peak of NRF1 surrounding the motif. Two primer sets, amplicon 1 and amplicon 2, for the rat genome were designed to detect H3K27ac enrichment and NRF1 binding, respectively, as shown in the track labelled 'Amplicons'. Conversion of genomic intervals of these amplicons was conducted using the UCSC liftOver tool to identify orthologous regions in the panels for mouse (mm9) and human (hg19). (**b**) The *Slc25a20* locus showed the increase in H3K27ac surrounding the TSS. Within this region, GABPA showed a localised binding to its motif both in humans and mice. Amplicon 3 was designed to detect GABPA binding and H3K27ac enrichment in the 5′ region in INS-1 cells, for which orthologous regions are indicated in the panels for mm9 and hg19. CD4, mouse CD4 T cells; Chr, chromosome; HepG2, Hep G2 human hepatoblastoma cell line; NP, neuronal progenitors; T47D, T47D human ductal breast cancer cell line

with control cells treated with scrambled siRNA, incubation in 3 mmol/l glucose resulted in increases in basal insulin secretion of 1.82-fold ($p < 0.001$; Fig. 6a), 3.09-fold ($p < 0.001$; Fig. 6b) and 2.35-fold ($p < 0.001$; Fig. 6c) in NRF1, MEF2A and GABPA knockdown cells, respectively. Another remarkable effect of the knockdown of these transcription factors was the reduction in insulin content at 3 mmol/l glucose, which was observed for the knockdown of MEF2A (33.9%; $p < 0.05$; Fig. 6e) and GABPA (26.6%; $p < 0.01$; Fig. 6f). In response to stimulation with 25 mmol/l glucose or 30 mmol/l KCl, there was no change in the secretory response of either MEF2A or GABPA knockdown cells (Fig. 6b,c), whereas 25 mmol/l glucose or 30 mmol/l KCl, respectively, caused a 14.0% ($p < 0.05$; Fig. 6a) increase and a 23.4% ($p < 0.01$; Fig. 6a) decrease in insulin secretion in NRF1 knockdown cells. In the present study, 48 h treatment with 0.5 mmol/l palmitate resulted in a significant increase in insulin secretion following incubation in 3 mmol/l glucose (1.44-fold, $p < 0.05$; Fig. 6a), along with a significant decrease in insulin content (35.6% reduction, $p < 0.05$; Fig. 6d), similar to the findings in the knockdown experiments. Furthermore, we observed a marked increase in both basal insulin secretion (3.36-fold; $p < 0.01$; Fig. 6a) and insulin response to 25 mmol/l glucose (1.36-fold, $p < 0.01$; Fig. 6a) in NRF1 knockdown cells treated with 0.5 mmol/l palmitate.

Discussion

In the present study, we show that the histone modification H3K27ac characteristic of active *cis*-regulatory regions changes purely through environmental effects by comparing samples derived from genetically identical C57BL/6J mice fed an HFD. Despite heterogeneity in the cellular composition, the global gene expression profile in pancreatic islets can be largely explained by that in beta cells [10], thus facilitating the analysis of whole islets and further examination of molecular mechanisms using INS-1 cells.

Previous large-scale analyses have demonstrated the correlation between changes in H3K27ac and gene expression [14]. Although transcription factors serve as direct transcriptional activators [38], they may also be involved in inducing

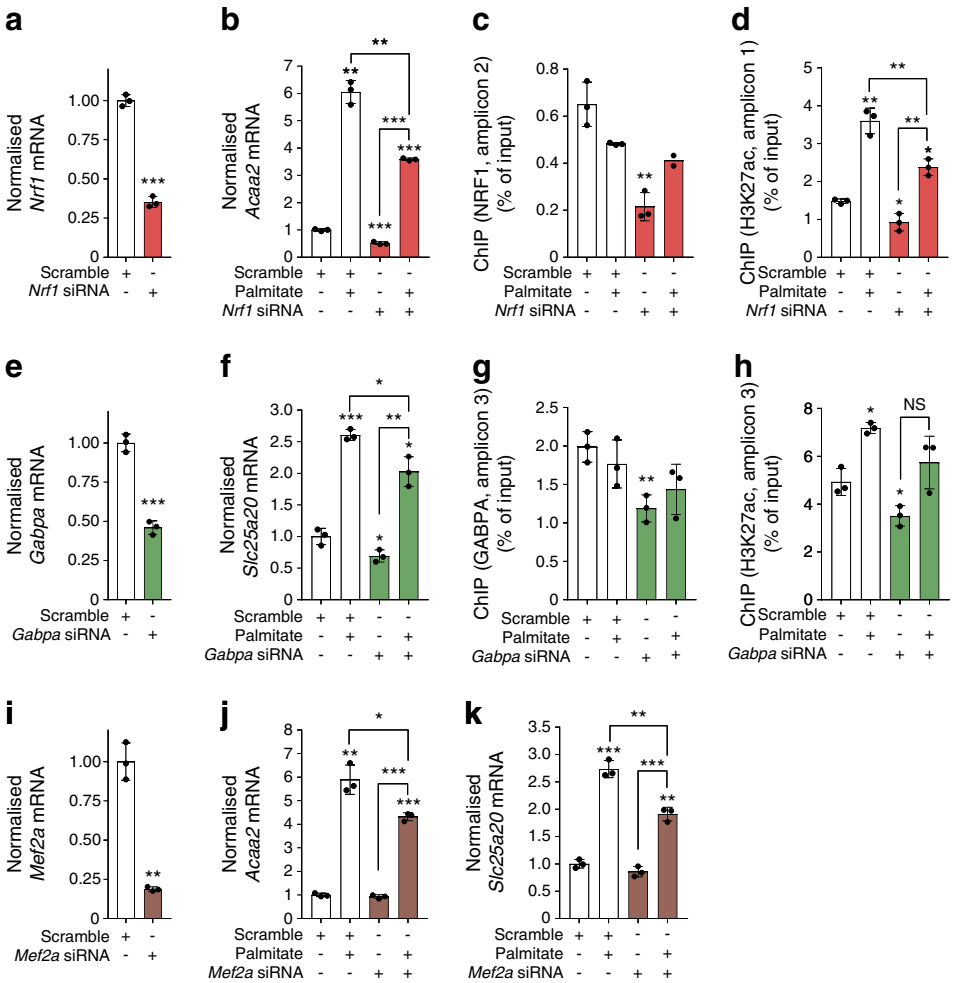

Fig. 5 Roles of NRF1, GABPA and MEF2A in gene expression and H3K27ac enrichment in basal and palmitate-treated INS-1 cells. Cells were initially treated with scrambled siRNA, *Nrf1* siRNA, *Gabpa* siRNA or *Mef2a* siRNA and treated 36 h later with vehicle or 0.5 mmol/l palmitate. (**a**–**d**) *Nrf1* siRNA treatment. Relative mRNA levels of *Nrf1* (**a**) and *Acaa2* (**b**) were measured after *Nrf1* siRNA treatment. Cells were subjected to ChIP using an anti-NRF1 antibody or IgG (control) (**c**). ChIP-enriched DNA was quantified by qPCR using primer pairs to detect NRF1 binding to *Acaa2* (amplicon 2 in Fig. 4) and *Nanog* promoter (negative control). Values are expressed as a percentage of input DNA. The displayed data show only results of amplicon 2 for NRF1 ChIP. H3K27ac ChIP-qPCR analysis was carried out (**d**). Enrichment within *Acaa2* promoter (amplicon 1 in Fig. 4) and *Nanog* promoter (negative control) is expressed as a percentage of input DNA. The displayed data show only results of amplicon 1 for H3K27ac ChIP. (**e**–**h**) *Gabpa* siRNA treatment. Relative mRNA levels of *Gabpa* (**e**) and *Slc25a20* (**f**) were measured after *Gabpa* siRNA treatment. Cells were subjected to ChIP using an anti-GABPA antibody or IgG (control) (**g**). ChIP-enriched DNA was quantified by qPCR with primer pairs to detect GABPA binding to *Slc25a20* (amplicon 3 in Fig. 4) and *Nanog* promoter (negative control). Values are expressed as a percentage of input DNA. The displayed data show only results of amplicon 3 for GABPA ChIP. H3K27ac ChIP-qPCR analysis was carried out (**h**). Enrichment within *Slc25a20* promoter (amplicon 3 in Fig. 4) and *Nanog* promoter (negative control) was expressed as a percentage of input DNA. The displayed data show only results of amplicon 3 for H3K27ac ChIP. (**i**–**k**) *Mef2a* siRNA treatment. Relative mRNA levels of *Mef2a* (**i**), *Acaa2* (**j**) and *Slc25a20* (**k**) were measured after *Mef2a* siRNA treatment. For all ChIP-qPCR analyses, all data, including those for IgG and *Nanog* promoter, are shown in ESM Fig. 8. Normalised mRNA levels were calculated relative to baseline, where *Actb* was used as an internal control. Data are shown as means ± SD, $n = 3$ (except for NRF1 ChIP of *Nrf1* siRNA and palmitate-treated samples, where $n = 2$.). *$p < 0.05$, **$p < 0.01$ and ***$p < 0.001$ compared with baseline or for comparisons indicated by horizontal line (calculated by two-sided unpaired *t* test)

epigenetic alterations in specific regions of the genome [18]. Consistent with this, our analyses revealed that environmental changes resulted in genome-wide epigenetic alterations, which correlated with differential gene expression. Furthermore, by de novo motif analysis, we identified enrichment of sequence motifs in H3K27ac regions showing changes in response to HFD, among which transcription factors such as NRF1, GABPA and MEF2A were the most enriched binding motifs. This led to the identification of potential target genes, *Acaa2* and *Slc25a20*, which are important for fatty acid β-oxidation. Our in vitro analysis using INS-1 cells produced results consistent with such in vivo findings. Suppression of NRF1, GABPA or MEF2A by siRNA resulted in blunted responses of both H3K27ac gain surrounding the TSS and gene induction to palmitate treatment, especially in the case of genes involved in fatty acid metabolism.

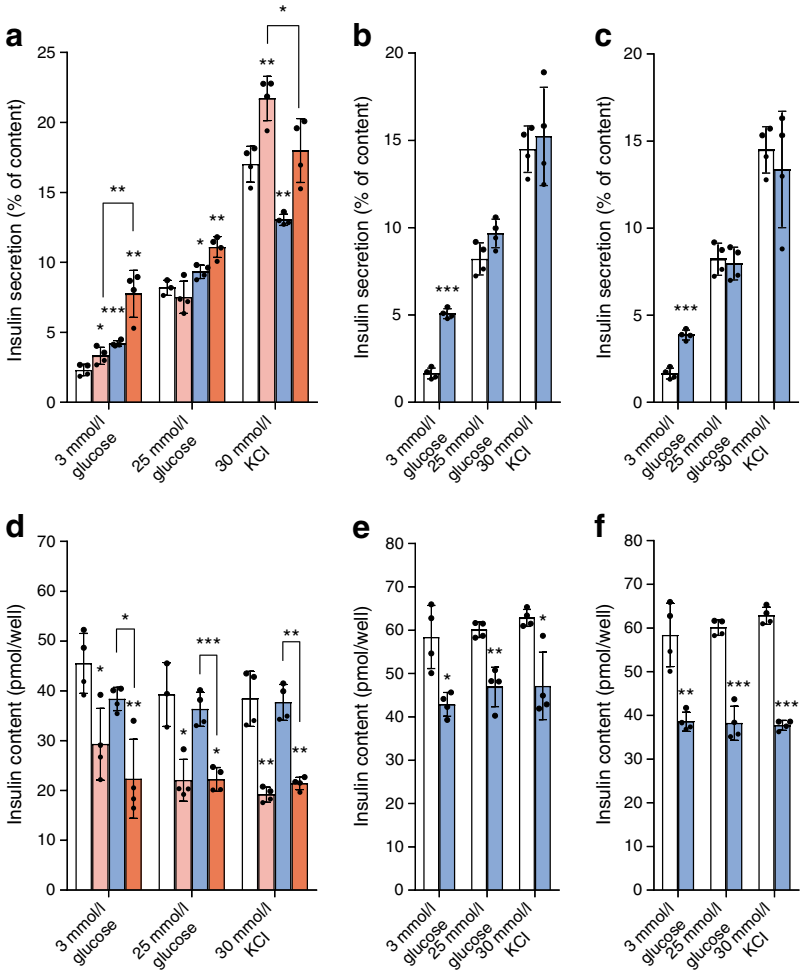

Fig. 6 GSIS and insulin content of INS-1 cells after siRNA-mediated knockdown of NRF1, MEF2A or GABPA. (**a**) GSIS in INS-1 cells after transfection of *Nrf1* siRNA; 0.5 mmol/l sodium palmitate was added 36 h after transfection. White bars, scrambled siRNA; pink bars, scrambled siRNA and palmitate; blue bars, *Nrf1* siRNA; orange bars, *Nrf1* siRNA and palmitate. (**b**) GSIS in INS-1 cells 72 h after transfection of *Mef2a* siRNA. White bars, scrambled siRNA; blue bars, *Mef2a* siRNA. (**c**) GSIS in INS-1 cells 72 h after transfection of *Gabpa* siRNA. White bars, scrambled siRNA; blue bars, *Gabpa* siRNA. (**d**) Total insulin content in INS-1 cells after transfection of *Nrf1* siRNA; 0.5 mmol/l sodium palmitate was added 36 h after transfection. White bars, scrambled siRNA; pink bars, scrambled siRNA and palmitate; blue bars, *Nrf1* siRNA; orange bars, *Nrf1* siRNA and palmitate. (**e**) Total insulin content in INS-1 cells after transfection of *Mef2a* siRNA. White bars, scrambled siRNA; blue bars, *Mef2a* siRNA. (**f**) Total insulin content in INS-1 cells after transfection of *Gabpa* siRNA. White bars, scrambled siRNA; blue bars, *Gabpa* siRNA. For each well, INS-1 cells were incubated in the indicated testing solution for 1 h to measure insulin secretion. Palmitate treatment was conducted for 48 h. $n = 4$. $^{*}p < 0.05$, $^{**}p < 0.01$ and $^{***}p < 0.001$ compared with baseline or for comparisons indicated by horizontal line (calculated by two-sided unpaired *t* test)

Therefore, the environmental factors, including fat-rich diet, shaped epigenetically induced specific pathways that were generated by the contribution of specific transcription factors.

NRF1, GABPA and MEF2A are transcription factors that have been linked to mitochondrial regulation [39]; however, their molecular function in pancreatic beta cells has not been well characterised. The knockdown experiments using INS-1 cells showed that changes in the secretory profile occurred in response to different testing solutions. This was in marked contrast to the reduced in vitro glucose responsiveness of pancreatic islets derived from 54-week-old hyperinsulinaemic DIO mice with mild glucose intolerance (ESM Fig. 9), in which the gene expression profile was similar to that of 37-week-old DIO mice (ESM Fig. 10). The epigenomic state should reflect the increased transcription factor activity (Table 1); thus, it could be possible that changing NRF1 activity could be useful in modulating pancreatic beta cell function. Besides this, the importance of the *NRF1* gene was shown by a recent GWAS demonstrating the association of an *NRF1* locus to the childhood obesity-related trait [40].

We also identified enrichment of a binding motif for MAFK in decreased H3K27ac regions. MAFK has been reported to be a negative regulator of pancreatic beta cell function and inhibition of endogenous small-MAFs improved glucose tolerance in DIO mice [41]. Therefore, our findings of

decreased H3K27ac regions could be responsible, at least in part, for mild glucose intolerance in DIO mice.

Our study supports the potential use of epigenetic analyses, such as H3K27ac, in a wide variety of applications for the research of human complex diseases. In this respect, the application of transcription factor-mediated repression of the epigenome has potential as an effective intervention against obesity and type 2 diabetes in the future.

Acknowledgements We thank C. B. Wollheim (Lund University, Lund, Sweden; University of Geneva, Geneva, Switzerland) and N. Sekine (University of Geneva) for providing INS-1 cells. We appreciate the assistance given by D. Suzuki, K. Nagase, N. Ishibashi (Lab Managers), H. Shiina and T. Shibuya (Administrative Assistants) (Department of Metabolic Disorder, National Center for Global Health and Medicine). We would like to thank Editage (www.editage.jp) for English language editing.

Data availability The next-generation sequencing data in the present study were deposited at ArrayExpress.
RNA-Seq:
Dataset name: ERR2538129 (Control), ERR2538130 (Diet-induced obesity)
Repository name and number: E-MTAB-6718 - RNA-Seq of pancreatic islets derived from mice fed a long-term high-fat diet against chow-fed controls.
ChIP-Seq:
Dataset name: ERR2538131 (Control), ERR2538132 (Diet-induced obesity)
Repository name and number: E-MTAB-6719 - H3K27ac ChIP-Seq of pancreatic islets derived from mice fed a long-term high-fat diet (HFD) against chow-fed controls.

Funding This work was supported by Japan Society for the Promotion of Science (JSPS) Grants-in-Aid for Scientific Research (KAKENHI), a grant from the National Center for Global Health and Medicine, the Japan Diabetes Foundation (to TN) and JSPS KAKENHI and a grant from the National Center for Global Health and Medicine (to KY). The study sponsors were not involved in the design of the study; the collection, analysis, and interpretation of data; writing the report; or the decision to submit the report for publication.

Duality of interest The authors declare that there is no duality of interest associated with this manuscript.

Contribution statement TN and KY conceived this study. TN and HU performed the experiments. TN performed the computational analyses. TN and KY wrote the manuscript. TN, HU, NF, MK, TU, MH, WN and KY analysed the data, interpreted the results and contributed to discussions. The manuscript was critically reviewed, revised and given final approval by all co-authors. TN and KY are the guarantors of this work.

References

1. Caspard H, Jabbour S, Hammar N, Fenici P, Sheehan JJ, Kosiborod M (2018) Recent trends in the prevalence of type 2 diabetes and the association with abdominal obesity lead to growing health disparities in the USA: an analysis of the NHANES surveys from 1999 to 2014. Diabetes Obes Metab 20(3):667–671. https://doi.org/10.1111/dom.13143
2. Flegal KM, Carroll MD, Ogden CL, Curtin LR (2010) Prevalence and trends in obesity among US adults, 1999-2008. JAMA 303(3):235–241. https://doi.org/10.1001/jama.2009.2014
3. Visscher PM, Wray NR, Zhang Q et al (2017) 10 Years of GWAS discovery: biology, function, and translation. Am J Hum Genet 101(1):5–22. https://doi.org/10.1016/j.ajhg.2017.06.005
4. Gaulton KJ, Nammo T, Pasquali L et al (2010) A map of open chromatin in human pancreatic islets. Nat Genet 42(3):255–259. https://doi.org/10.1038/ng.530
5. Maurano MT, Humbert R, Rynes E et al (2012) Systematic localization of common disease-associated variation in regulatory DNA. Science 337(6099):1190–1195. https://doi.org/10.1126/science.1222794
6. Farh KK, Marson A, Zhu J et al (2015) Genetic and epigenetic fine mapping of causal autoimmune disease variants. Nature 518(7539):337–343. https://doi.org/10.1038/nature13835
7. Kahn SE, Hull RL, Utzschneider KM (2006) Mechanisms linking obesity to insulin resistance and type 2 diabetes. Nature 444(7121):840–846. https://doi.org/10.1038/nature05482
8. Kulkarni RN, Stewart AF (2014) Summary of the Keystone islet workshop (April 2014): the increasing demand for human islet availability in diabetes research. Diabetes 63(12):3979–3981. https://doi.org/10.2337/db14-1303
9. Stitzel ML, Sethupathy P, Pearson DS et al (2010) Global epigenomic analysis of primary human pancreatic islets provides insights into type 2 diabetes susceptibility loci. Cell Metab 12(5):443–455. https://doi.org/10.1016/j.cmet.2010.09.012
10. Nica AC, Ongen H, Irminger JC et al (2013) Cell-type, allelic, and genetic signatures in the human pancreatic beta cell transcriptome. Genome Res 23(9):1554–1562. https://doi.org/10.1101/gr.150706.112
11. Pasquali L, Gaulton KJ, Rodríguez-Seguí SA et al (2014) Pancreatic islet enhancer clusters enriched in type 2 diabetes risk-associated variants. Nat Genet 46(2):136–143. https://doi.org/10.1038/ng.2870
12. Rada-Iglesias A, Bajpai R, Swigut T, Brugmann SA, Flynn RA, Wysocka J (2011) A unique chromatin signature uncovers early developmental enhancers in humans. Nature 470(7333):279–283. https://doi.org/10.1038/nature09692
13. Cheng Y, Ma Z, Kim BH et al (2014) Principles of regulatory information conservation between mouse and human. Nature 515(7527):371–375. https://doi.org/10.1038/nature13985
14. Gjoneska E, Pfenning AR, Mathys H et al (2015) Conserved epigenomic signals in mice and humans reveal immune basis of Alzheimer's disease. Nature 518(7539):365–369. https://doi.org/10.1038/nature14252
15. Carrer A, Parris JL, Trefely S et al (2017) Impact of a high-fat diet on tissue acyl-coA and histone acetylation levels. J Biol Chem 292(8):3312–3322. https://doi.org/10.1074/jbc.M116.750620
16. Malmgren S, Spégel P, Danielsson AP et al (2013) Coordinate changes in histone modifications, mRNA levels, and metabolite profiles in clonal INS-1 832/13 β-cells accompany functional adaptations to lipotoxicity. J Biol Chem 288(17):11973–11987. https://doi.org/10.1074/jbc.M112.422527
17. Siersbæk M, Varticovski L, Yang S et al (2017) High fat diet-induced changes of mouse hepatic transcription and enhancer activity can be reversed by subsequent weight loss. Sci Rep 7(1):40220. https://doi.org/10.1038/srep40220
18. Zaret KS (2018) Pioneering the chromatin landscape. Nat Genet 50(2):167–169. https://doi.org/10.1038/s41588-017-0038-z
19. Nishimura W, Eto K, Miki A et al (2013) Quantitative assessment of Pdx1 promoter activity in vivo using a secreted luciferase reporter system. Endocrinology 154(11):4388–4395. https://doi.org/10.1210/en.2012-2248

20. Anders S, Huber W (2010) Differential expression analysis for sequence count data. Genome Biol 11(10):R106. https://doi.org/10.1186/gb-2010-11-10-r106
21. Sun J, Nishiyama T, Shimizu K, Kadota K (2013) TCC: an R package for comparing tag count data with robust normalization strategies. BMC Bioinformatics 14(1):219. https://doi.org/10.1186/1471-2105-14-219
22. Huang DW, Sherman BT, Lempicki RA (2009) Systematic and integrative analysis of large gene lists using DAVID Bioinformatics Resources. Nat Protoc 4(1):44–57. https://doi.org/10.1038/nprot.2008.211
23. Robinson JT, Thorvaldsdóttir H, Winckler W et al (2011) Integrative genomics viewer. Nat Biotechnol 29(1):24–26. https://doi.org/10.1038/nbt.1754
24. Zang C, Schones DE, Zeng C, Cui K, Zhao K, Peng W (2009) A clustering approach for identification of enriched domains from histone modification ChIP-Seq data. Bioinformatics 25(15):1952–1958. https://doi.org/10.1093/bioinformatics/btp340
25. Heinz S, Benner C, Spann N et al (2010) Simple combinations of lineage-determining transcription factors prime *cis*-regulatory elements required for macrophage and B cell identities. Mol Cell 38(4):576–589. https://doi.org/10.1016/j.molcel.2010.05.004
26. Love MI, Huber W, Anders S (2014) Moderated estimation of fold change and dispersion for RNA-seq data with DESeq2. Genome Biol 15(12):550. https://doi.org/10.1186/s13059-014-0550-8
27. Ogata H, Goto S, Sato K, Fujibuchi W, Bono H, Kanehisa M (1999) KEGG: Kyoto Encyclopedia of Genes and Genomes. Nucleic Acids Res 27(1):29–34. https://doi.org/10.1093/nar/27.1.29
28. Clee SM, Attie AD (2007) The genetic landscape of type 2 diabetes in mice. Endocr Rev 28(1):48–83. https://doi.org/10.1210/er.2006-0035
29. Sharma RB, O'Donnell AC, Stamateris RE et al (2015) Insulin demand regulates β cell number via the unfolded protein response. J Clin Invest 125(10):3831–3846. https://doi.org/10.1172/JCI79264
30. Dekker J, Rippe K, Dekker M, Kleckner N (2002) Capturing chromosome conformation. Science 295(5558):1306–1311. https://doi.org/10.1126/science.1067799
31. McLean CY, Bristor D, Hiller M et al (2010) GREAT improves functional interpretation of cis-regulatory regions. Nat Biotechnol 28(5):495–501. https://doi.org/10.1038/nbt.1630
32. Smith SB, Qu HQ, Taleb N et al (2010) Rfx6 directs islet formation and insulin production in mice and humans. Nature 463(7282):775–780. https://doi.org/10.1038/nature08748
33. Gaulton KJ, Ferreira T, Lee Y et al (2015) Genetic fine mapping and genomic annotation defines causal mechanisms at type 2 diabetes susceptibility loci. Nat Genet 47(12):1415–1425. https://doi.org/10.1038/ng.3437
34. Yamagata K, Oda N, Kaisaki PJ et al (1996) Mutations in the hepatocyte nuclear factor-1alpha gene in maturity-onset diabetes of the young (MODY3). Nature 384(6608):455–458. https://doi.org/10.1038/384455a0
35. Busch AK, Gurisik E, Cordery DV et al (2005) Increased fatty acid desaturation and enhanced expression of stearoyl coenzyme A desaturase protects pancreatic β-cells from lipoapoptosis. Diabetes 54(10):2917–2924. https://doi.org/10.2337/diabetes.54.10.2917
36. Soni MS, Rabaglia ME, Bhatnagar S et al (2014) Downregulation of carnitine acyl-carnitine translocase by miRNAs 132 and 212 amplifies glucose-stimulated insulin secretion. Diabetes 63(11):3805–3814. https://doi.org/10.2337/db13-1677
37. Brun T, Scarcia P, Li N et al (2013) Changes in mitochondrial carriers exhibit stress-specific signatures in INS-1E β-cells exposed to glucose versus fatty acids. PLoS One 8(12):e82364. https://doi.org/10.1371/journal.pone.0082364
38. Lambert SA, Jolma A, Campitelli LF et al (2018) The human transcription factors. Cell 172(4):650–665. https://doi.org/10.1016/j.cell.2018.01.029
39. Scarpulla RC (2008) Transcriptional paradigms in mammalian mitochondrial biogenesis and function. Physiol Rev 88(2):611–638. https://doi.org/10.1152/physrev.00025.2007
40. Comuzzie AG, Cole SA, Laston SL et al (2012) Novel genetic loci identified for the pathophysiology of childhood obesity in the Hispanic population. PLoS One 7(12):e51954. https://doi.org/10.1371/journal.pone.0051954
41. Nomoto H, Kondo T, Miyoshi H et al (2015) Inhibition of small Maf function in pancreatic β-cells improves glucose tolerance through the enhancement of insulin gene transcription and insulin secretion. Endocrinology 156(10):3570–3580. https://doi.org/10.1210/en.2014-1906